SANDIA REPORT

SAND2016-10174
Unlimited Release
September 2016

Novel Materials and Devices for Solid-State Neutron Detection

Kent B. Pfeifer[1], Komandoor E. Achyuthan[1], Matthew Allen[2], Michele L. B. Denton[3], Michael P. Siegal[4], and Ronald P. Manginell[1]

[1]Bio/Chem/Physical MicroSensors Department
[2]Technical Analysis Department
[3]AUR Sys Engineering Department
[4]Nanoscale Sciences Department

Sandia National Laboratories
Albuquerque, NM 87185 USA

Prepared by
Sandia National Laboratories
Albuquerque, New Mexico 87185 and Livermore, California 94550

Sandia National Laboratories is a multi-mission laboratory managed and operated by Sandia Corporation, a wholly owned subsidiary of Lockheed Martin Corporation, for the U.S. Department of Energy's National Nuclear Security Administration under contract DE-AC04-94AL85000.

Issued by Sandia National Laboratories, operated for the United States Department of Energy by Sandia Corporation.

Available to DOE and DOE contractors from
U.S. Department of Energy
Office of Scientific and Technical Information
P.O. Box 62
Oak Ridge, TN 37831

Telephone: (865) 576-8401
Facsimile: (865) 576-5728
E-Mail: reports@osti.gov
Online ordering: http://www.osti.gov/scitech

Available to the public from
U.S. Department of Commerce
National Technical Information Service
5301 Shawnee Rd
Alexandria, VA 22312

Telephone: (800) 553-6847
Facsimile: (703) 605-6900
E-Mail: orders@ntis.gov
Online order: http://www.ntis.gov/search

SAND2016-10174
Unlimited Release
September 2016

Novel Materials and Devices for Solid-State Neutron Detection

Kent B. Pfeifer[1], Komandoor E. Achyuthan[1], Matthew Allen[2],
Michele L. B. Denton[3], Michael P. Siegal[4], and Ronald P. Manginell[1]

[1]Bio/Chem/Physical MicroSensors Department
[2]Technical Analysis Department
[3]AUR Sys Engineering Department
[4]Nanoscale Sciences Department
Sandia National Laboratories
P.O. Box 5800
Albuquerque, New Mexico 87185-MS1425

ABSTRACT

Neutron sensing is critical in civilian, military, industrial, biological, medical, basic research, and environmental applications. Conventional neutron sensors are limited by size, weight, cost, portability, and helium supply. Here the microfabrication of Gd conversion material-based heterojunction diodes is described for detecting thermal neutrons using electrical signals produced by internal conversion electrons (ICE). Films with negligible stress were produced at the tensile-compressive crossover point, enabling Gd coatings of any desired thickness by controlling the radiofrequency sputtering power and using the zero-point near p(Ar) of 50 mTorr at 100 W. Post-deposition Gd oxidation-induced spallation was eliminated by growing a residual stress-free 50 nm neodymium-doped aluminum cap layer atop Gd. Resultant coatings were stable for at least six years demonstrating excellent product shelf life. Depositing Gd on the diode surface eliminated air gap, leading to improved efficiency and facilitating monolithic microfabrication. The conversion electron spectrum was dominated by ICE with energies of 72, 132, and 174 keV. Results are reported on neutron reflection and moderation by polyethylene for enhanced sensitivity and γ- and X-ray elimination for improved specificity. Optimal Gd thickness was 10.4 μm with 300 μm thick partially depleted diode of 300 mm2 active surface area. Fast detection within 10 minutes at a neutron source-to-diode distance of 11.7 cm was achieved using this configuration. All ICE energies along with γ-ray and Kα X-ray were modeled to emphasize correlations between experiment and theory and to calculate efficiencies. Semiconductor thermal neutron detectors offer advantages for field-sensing of radioactive neutron sources.

ACKNOWLEDGEMENTS

Sandia National Laboratories is a multi-program laboratory operated by Sandia Corporation, a wholly owned subsidiary of Lockheed Martin Company, for the U.S. Department of Energy's National Nuclear Security Administration under contract DE-AC04-94AL85000. We thank Edward Cole, David Wheeler, Robert Koudelka, and Lyle Brunke for productive interactions and materials support.

Contents

FIGURES

1. INTRODUCTION

Neutrons are subatomic neutral nuclear particles without net electrical charge. Based on their energies, neutrons are classified as fast (1-20 MeV, ~5 x 10^7 m/s), slow (1-10 eV, ~4 x 10^4 m/s), and thermal (~0.025 eV, ~2 x 10^3 m/s). Neutrons are weakly affected by electromagnetic fields and do not interact by Coulombic forces. Neutron detection is thus, an indirect process from their reactions with nuclei in other elements ("conversion materials"), which generate energetic charged particles that can be detected by their electrical signal. For example, gadolinium (Gd)

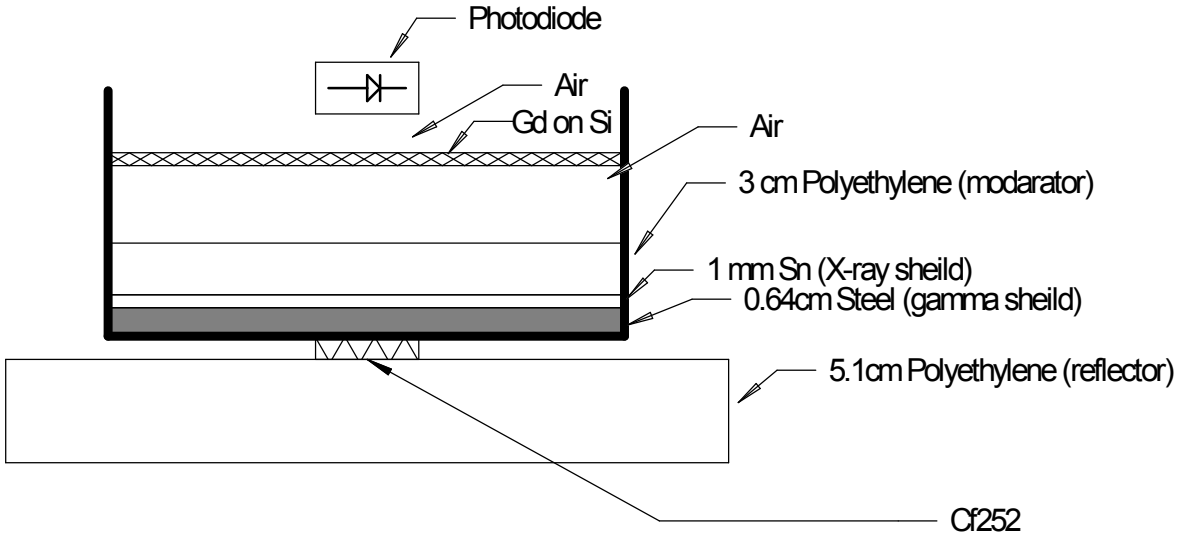

Figure 1. Schematic of the experimental setup showing the ^{252}Cf source, HDPE moderator, steel and Sn for γ/X-ray shielding, Gd film and the PIN diode detector.

neutron capture reaction results in the emission of prompt gamma rays (γ-rays), internal conversion electrons (ICE), Auger-Coster-Kronig (ACK) electrons, and X-rays [1, 2], all of which are detectable.

Neutron sensors have civilian, medical, scientific, industrial, and military applications. For example, low-dose rate (LDR) neutron brachytherapy is used against cancers.[3] In Gd-neutron capture therapy (NCT) [4], ICE play an important role.[5, 6] The complex emissions from Gd conversion require careful dosimetry [7], especially with biological effects such as neutron-induced bystander effects (NIBE) and neutron radioadaptive response (RAR).[8, 9] Personal or environmental monitoring detects an increase in neutron levels due to an event, either accidental [10-12] or human intent.[13] Although background neutron levels are small, certain individuals have higher than normal neutron radiation exposure potential such as medical personnel (and patients) in cancer therapy, airline crews, oil workers, and employees of nuclear power plants and reactors.[9, 14, 15] Consequently, there is interest in robust, inexpensive neutron sensing.[16]

Neutron-induced fission ("neutron activation") is used in nuclear reactors and nuclear weapons

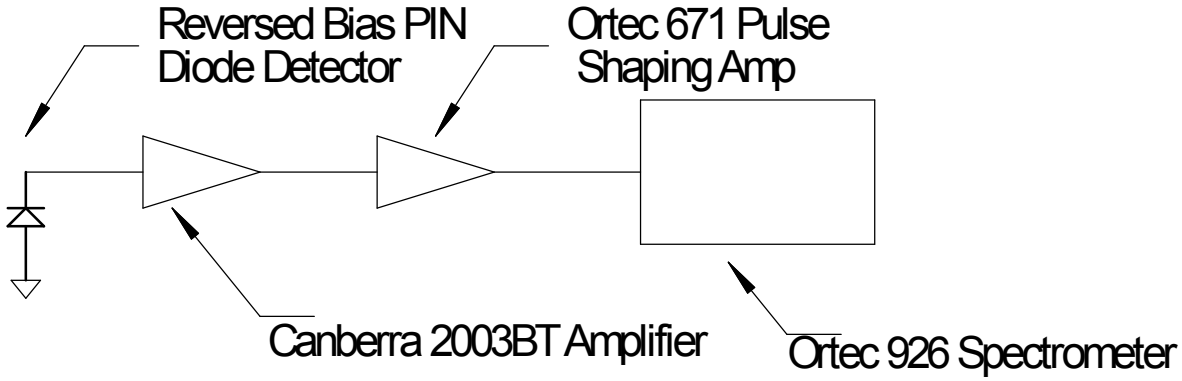

Figure 2. Schematic of the detection instruments to measure electron energies. Electrons were detected as a current change in the PIN diode after amplification by a Canberra preamplifier. The electronic pulse was then shaped by the ORTEC amplifier and the electrons were counted as a function of energy using the ORTEC spectrometer.

(NWs). Plutonium-239 (^{239}Pu) and uranium-233, 235 (^{233,235}U) are special nuclear materials (SNM) and sources of spontaneous fission neutrons in NWs. The detection of SNM is critical for nuclear non-proliferation and national security to track cargo for SNM at ports-of-entry. The low-energy γ-rays of SNM can be blocked, preventing detection. The α-particles with a large linear energy transfer (LET) do not travel further than ~2 inches (~5.08 cm) in air. Since neutrons penetrate γ-ray absorbers, detecting an increase in neutron level would be indicative of SNM.

Finally, the trivalent actinide ^{252}Californium (^{252}Cf) is a neutron emitting radioisotope that is used in clinical brachytherapy and NCT.[17, 18] It is a high neutron emitter (3.768 neutrons/spontaneous fission, 3.1% decay probability, and neutron yield of 2.314 x 10^{12} neutron/g/sec), with a relatively long half-life of 2.645 years.[19] The majority (96.9%) of ^{252}Cf undergoes α-decay, losing two protons and two neutrons, transforming into Curium-248 (^{248}Cm). Due to encapsulation, Helium-4 (^{4}He) nuclei do not escape the package. A small (3.092%) portion of ^{252}Cf decays by spontaneous fission, producing neutrons, prompt γ-rays, and photons.[20] Thus, there is an interest in ^{252}Cf neutron emission in medicine.

Conventional neutron detectors use tritium's (^{3}H) decay product Helium-3 (^{3}He), which has a reasonable cross-section for thermal neutrons. Parenthetically, mass attenuation coefficient, which refers to neutron penetration, is defined as μ/ρ (attenuation coefficient/density, m^2/kg). Since the numerator has units of length squared (m^2), it is referred to as a "cross-section." Cross-sections do not represent a physical area, but the probability of an interaction expressed in units of "barns" where, 1 barn = 10^{-28} m^2. In addition to a global shortage of ^{3}H due to applications in national security, nonproliferation, and medical diagnostics, ^{3}He detectors suffer from issues of availability, portability, high-bias voltage (1200 to 1800 V), and cost.[21] Semiconductor devices (semiconductor diodes, solid-state detectors) are potential replacements for ^{3}He neutron detectors. In this paper, the microfabrication of Gd-converters on

silicon-based diodes is described for detecting thermal neutrons from the electrical signals of ICE. Results are reported on neutron moderation, γ-ray elimination, sensitivity, specificity, and speed of neutron detection. The data are modeled after earlier mathematical studies to emphasize correlations. A semiconductor portable thermal neutron detector is suitable for field-sensing of neutron sources and patient bedside monitoring.

2. MATERIALS AND METHODS

Neutron source

The neutron source was a sealed container of ^{252}Cf (Serial # 1534, RS # 2852) available from the radiological laboratory at Sandia National Laboratories (SNL). At the time of the experiments,

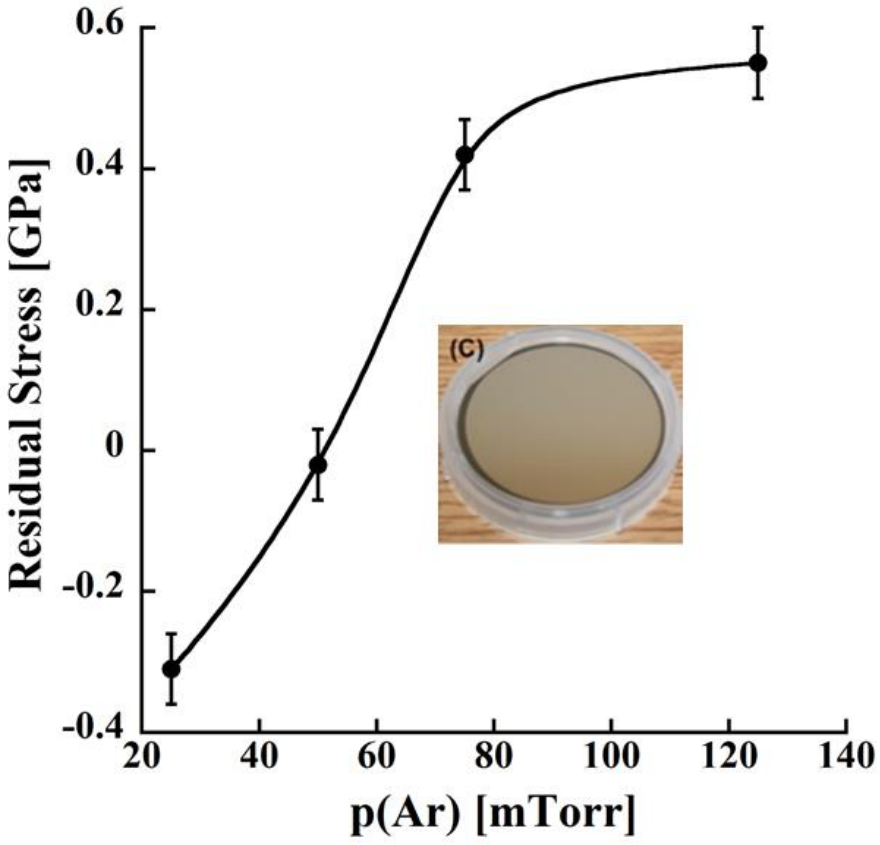

Figure 3. Residual stress of 500 nm thick Gd films on Si(100) deposited at a constant 100 W RF sputter power as a function of Ar total pressure. All films were coated with a 50 nm thick protective layer of Nd-doped Al to prevent unwanted oxidation of Gd. A smooth curve fitting was used to profile the data with the Kaleidagraph program (Synergy Software, Reading, PA, USA). Inset shows a photograph of the conversion (C) material with Nd-doped Al capping layer to eliminate post-deposition, oxidation-induced Gd degradation [35].

the ^{252}CF source had an activity of 38.4 μCi, contained within a cylindrical package of 25 mm in length and 12.5 mm in diameter. The neutron sensor devices were characterized using this sealed neutron emitter.

Gadolinium (Gd)

Natural Gd used in this work was purchased from Plasmaterials (Livermore, CA) in the form of a 2" (5.08 cm) diameter, 0.125" (~0.32 cm) thick sputter target. The material is natural Gd with a purity of 99.9%. The rare earth metal element was used as received.

Microfabrication

The Gd films were grown on 500 μm thick silicon (100) (Si(100)) substrates or photodiodes using a radiofrequency (RF) sputter deposition technique.[22] During sputtering, Gd and the electrodes were under vacuum and the inert gas argon (Ar) was introduced into the vacuum chamber as background. The RF power source was used to ionize Ar. The Gd target was bombarded by high-energy Ar ions, generating Gd ions which then condensed on the substrate as a thin-film of the desired thickness. Residual film stress was determined by measuring the change in curvature of a two-inch Si(100) wafer using a stylus profilometer before and after deposition of Gd. Optimal area of uniform thickness was achieved by slowly rotating the substrate during the deposition process. Since deposition rate is almost linearly proportional to RF power, Gd film deposition was carried out at 100 W power. Post-deposition of Gd oxidation-induced spallation (peeling, flaking) was eliminated by growing a residual stress-free 50 nm neodymium (Nd)-doped aluminum (Al) cap layer atop the Gd film. All Gd depositions were performed in the absence of any type of adhesion layers on the substrate.

Neutron Detection System

Testing and evaluation of the conversion of moderated neutrons into electrons by Gd was accomplished using the detector system illustrated in Figure 2. It consists of ^{252}Cf neutron source sitting atop a 5.1 cm polyethylene reflector. The neutron source was then progressively layered by 0.64 cm steel, 0.1 cm tin, 3 cm polyethylene moderator, and a 4 cm air-gap, before the placement of 10 μm Gd-coated 500 μm thick silicon wafer below the diode. This diagram illustrates the experimental set-up for the uncoated diodes using the Gd on Si wafer electron capture technique. For the Gd coated diodes, the wafer is removed as the Gd is coated directly onto the diode.

Partially Depleted (PD) Diodes

The electrons produced by neutron capture of Gd were measured by Canberra Si diodes (Canberra Industries, Inc., Meriden, CT, USA). These are partially depleted (PD), passivated, implanted, planar, silicon (PIPS) charged particle detectors with an implanted barrier contact that forms a thin abrupt junction. The diodes were in metal housings with entrance window <50 nm for improved resolution, and 100-1000 μm depletion regions sufficient to stop 0.01-0.3 MeV ICE. The rugged PIPS detectors were fabricated by planar processing using photolithographic techniques for defining device geometries. The PIPS detectors have leakage current that is typically 1/8-1/100 of silicon surface barrier (SSB) or diffused junction (DJ) detectors and low-reverse current translating into low-noise. Size scaling was accomplished by various diode configurations, all devices were 300 mm^2 active area, with 100-500 μm thicknesses and reverse-bias operating voltages of -40 V for 100 μm, -60 V for 300 μm, and -100 V for 500 μm diodes.

Electron Nuclear Spectroscopy

Detection of the electrons was accomplished using the electronic system illustrated in Figure 2. The detection system consisted of amplification of the Canberra diode response to the incoming conversion electrons from Gd. Diode response was amplified using a Canberra 2003 BT preamplifier which operates as a charge-to-voltage converter (0.45 V/pC; bias to ± 1 kV). The current pulse was then Gaussian shaped by the ORTEC 671 amplifier (ORTEC, Oak Ridge, TN, USA) designed for use with Si-charged particle detectors to allow analysis of the energy by the pulse-shaping system and the ORTEC 926 spectrometer fitted with an analog-to-digital converter (ADC) board and Universal Serial Bus (USB) interface. This Multichannel Buffer (MCB) equipment is a Nuclear Instrumentation Module (NIM) module was designed for high-performance data acquisition in electron nuclear spectroscopy applications. The resulting spectrum was analyzed using the ORTEC *Maestro* MultiChannel Analyzer (MCA) Emulation Software. The final output is directly proportional to the collected charge.

Measurements

The measurements of the individual diodes and Gd films were made using the following general procedure. First, after assembly of the system without the Gd film, a ^{57}Co source (8.88 x 10^{-2} μCi) and ^{241}Am (9.68 μCi) source were inserted directly below the PIN diode for calibration. The ORTEC *Maestro* software was then configured to correctly identify the energy of the 59.9 keV γ from the ^{241}Am and the 122 keV and 136 keV γ-rays from the ^{57}Co source. Next, the ^{241}Am and the ^{57}Co sources were removed and the ^{252}Cf source was placed as shown in Figure 1, again without the Gd film. This was to produce a background measurement of the response over the energy range of interest. As the detector is sensitive to γ-radiation as well as electrons, this was required to subtract background radiation. Thus, the measured electronic signal was directly proportional to the incident neutron flux. Next, various thicknesses of Gd films were used and the measurement was repeated. Data were collected and stored for several diode thicknesses and for several integration times from 10 to 60 min. Additionally, a measurement was made with the same system including the Gd film with a 0.025 mm Al layer between the Gd film and the PIN diode. The Al film was grounded to shunt any electrons from Gd to the detector as verification that the signal was due to electrons rather than from another γ source.

Modeling and Efficiency Calculations

Modeling of thermal neutron flux was carried out with Geometry ANd Tracking (GEANT4). The software and source code are available from http://geant4.org/geant4/index.shtml. The software simulation toolkit is for modeling both the detector and the physics of the passage of particles through matter.[23] It provides an object-oriented technology and follows an iterative incremental software process. Since GEANT4 is a toolkit, an extensive collection of data libraries and C++ classes exist. The user is expected to build their own application for running simulations in GEANT4. In modeling the neutron source, parameters were set up to get as close as possible to the experimental conditions. The neutron flux was calculated as described in the Results and Discussion section and converted to the actual number of neutrons by multiplying it for the specified measurement duration. Energy deposited in the Si layer (charged particle detector) was recorded and the data were presented in a histogram format.

3. RESULTS AND DISCUSSIONS

Neutron Signal

The capture of thermal neutrons by natural Gd produces conversion electrons at several different energies that can be detected by a PIN diode. A PIN diode has a wide, undoped intrinsic semiconductor region (*i.e.,* a larger depletion region, unlike PN diodes) that is flanked by doped *p*- and *n*-type semiconductors for ohmic contacts.[24] The PIN diode enhances charge collection efficiency and response time of the planar conversion layer detector. The primary electron energies are approximately 72 keV, 132 keV, and 174 keV. These electrons are ionized from the *K* and *L* shells of Gd atoms[25] as follows:

$$^{155}Gd(15\%) + n \rightarrow {}^{156}Gd + \gamma(0.09, 0.20\ and\ 0.30keV) + X\text{–}ray + ACK + ICE \text{ * MERGEFORMAT (1)}$$

$$^{157}Gd(16\%) + n \rightarrow {}^{158}Gd + \gamma(0.08, 0.18\ and\ 0.28keV) + X\text{–}ray + ACK + ICE \text{ * MERGEFORMAT (2)}$$

In 39% of neutron capture by Gd, ICE with energy mainly of 72 keV (*L* shell) are emitted, where the conversion efficiency can reach up to 30%.[26] The ^{252}Cf neutron source used here undergoes spontaneous α-decay fission with the loss of two protons and two neutrons [19]. The neutron flux *n* for this source was calculated as, $n = A$ (3.7 x 10^{10} Bq/Ci) (s.f.) ν, where *A* is the neutron activity in Ci (34.5 x 10^{10} Bq/second), s. f. is the branching ratio for spontaneous fission (0.03092), and ν is the average number of neutrons per fission (3.768). Using these values, a neutron flux of 1.487 x 10^5 neutrons/second was calculated. This level of neutron activity was sufficient to generate measurements within an experimental timeframe.

Choice of Gd

The naturally occurring rare earth metal element used here as a neutron conversion material was Gd which is composed of several stable isotopes: ^{154}Gd, ^{155}Gd, ^{156}Gd, ^{157}Gd, ^{158}Gd, and ^{160}Gd. Of these, ^{157}Gd and ^{155}Gd have the largest thermal neutron capture cross-sections of any stable isotope: 255,000 barns and 65,000 barns respectively [2, 26, 27], which permit fast capture with smaller spatial separation, thereby reducing background. The two isotopes provide approximately 30% abundance in natural Gd (14.8% ^{155}Gd and 15.7% ^{157}Gd), with an average effective cross-cross-section of 49,000 barns, compared to 5300 barns for ^{3}He. These statistics permitted the use of natural Gd instead of the expensive ^{157}Gd.[28]

Microfabrication

Oxidation-free, stable Gd films of uniform and precise thicknesses are critical for neutron sensing. This was achieved within the cleanroom facilities of the Microsystems & Engineering Sciences Applications (MESA) complex at Sandia National Labs. Microfabrication enables rapid, consistent and large-volume manufacturing capabilities with the solid-surface providing greater coverage area for Gd conversion material.[29] Radio frequency (RF) sputtering is a technique for depositing thin-films of uniform thickness upon substrates [22]. The deposition of Gd films several microns thick upon a substrate surface is not trivial since residual stress is a problem caused by the energetic physical deposition process. These stresses limit the critical thickness to less than 1 μm, above which the films begin to delaminate. Two deposition parameters were used to examine and control film stress from tensile to compressive during sputter deposition. These were Ar sputter pressure and RF sputter power, which attenuate the

kinetic energy of the depositing species while it migrates from target to the substrate.[30] As Ar pressure increases, kinetic energy of the depositing species decreases, resulting in lower residual tensile stress, until it crosses zero and turns compressive. However, higher Ar pressure lowers the Gd deposition rate, which is relevant when considering the timeframe for the deposition of films up to 100 μm thickness.

Since deposition rate is (nearly) linearly proportional to RF power, the deposition of Gd films at 100 W power was studied. The profile presented in Figure 3 shows the results for 500 nm thick Gd films capped with 50 nm Nd-doped Al. A monotonic progression of the residual film stress from tensile to compressive with increasing Ar pressure during film deposition was observed. At high pressures (120 mTorr, Figure 3), a flattening of stress was seen, indicative of the Gd film buckling and the films had a cloudy appearance. Such undesirable effects were eliminated and films with negligible stress were produced at the tensile-compressive crossover (zero) point, enabling coatings of any desired thickness by controlling the RF sputtering power and using the zero-point crossover near *p*(Ar) of 50 mTorr (Figure 3) to produce uniform Gd films. The films exhibited a highly polished mirror-like shiny appearance of a smooth surface. Profilometer measurements of curvature before and after Gd film deposition showed no changes, indicative of essentially zero-stress Gd films. The films did not exhibit spallation (peeling, flaking) or delamination at various thicknesses (3-20 μm). Empirical data including evidence of smooth, shiny, polished, mirror-like appearance of the conversion material demonstrated that such coatings were stable for at least six years with no signs of degradation. Thus, the low stress, oxidation-free (due to Nd-doped Al cap layer) Gd films of any desired thickness, and excellent product shelf life, were all ideal for use in a neutron sensor.

Detector Setup

There were several important points regarding the detector setup and these are described next. First, γ-rays are ubiquitous in the background[29] arising from the X-ray ambient background caused by γ-radiation scattering including Compton scattering.[1] This situation is exacerbated when compared to the low natural neutron background fluence. There are two sources contributing to γ-ray background: external γ-rays accompanying ^{252}Cf and internal prompt γ-rays[31] (Eq. * MERGEFORMAT (1) and * MERGEFORMAT (2) above) due to Gd's (Z = 64) high probability of interaction that produces moderate energy electrons by Compton, photoelectric and electron-positron pair processes[32]. These factors make it easy to record false positives whilst detecting SNM since an electron from γ-interaction is not easily distinguished from ICE. The problem was overcome during device construction by using relatively thin (100-500 μm) silicon wafers which were expected to have low sensitivity to γ-rays.[33] The γ-ray rejection (γ-blindness) was further ensured by positioning a steel layer between the neutron source and the diode

Next, the ~200 keV γ-photons produced by ^{252}Cf at the rate of 1.4 x 10^2 R/(hr-gm) at one meter, were filtered by the steel plate. Since all neutrons are born at fast energies (MeV), significant moderation is required to achieve a high probability of capture reactions. The most probable neutron energy of ^{252}Cf is 0.7 MeV with an average energy of 2.1 MeV.[19] The conversion cross-section of natural Gd to such high energy neutrons is about a million fold lower compared to the energy of thermal neutrons (0.026 eV).[29] Therefore, a moderator was employed to slow

the high energy neutrons by using hydrogen-rich polymers such as the high-density polyethylene (HDPE) layer between ^{252}Cf and the detector (Figure 1).[29]

The ~2 MeV neutrons produced by ^{252}Cf (4.4 x 10^9 neutrons/(sec-Ci)) which for the 38.4 μCi cylindrical source employed here equaled ~1.7 x 10^5 neutrons/sec total. However, since the source dimension was ~12.5 mm cylinder, the total neutron flux that intersects the 12.5 mm diameter detector was significantly less. A planar geometry limits the reaction products reaching the detector since the charged particles are emitted in all directions.[32] In order to improve the efficiency of the system, a polyethylene layer was placed beneath the source to reflect neutrons back towards the detector (Fig. 1). A tin (Sn) layer was placed above the steel to filter the additional X-rays that were formed during γ-filtering in the steel. Now the moderated ~0.1 eV neutrons[34] travelled through an air layer before finally reaching the Gd-coated silicon (Si) wafer. The total source to-detector-distance was 11.7 cm, close to the 10.6 cm reported previously.[29] Since the distance between the Gd converter and the Si detector is critical in determining efficiency and an air-gap could cause sensitivity losses, the current approach of

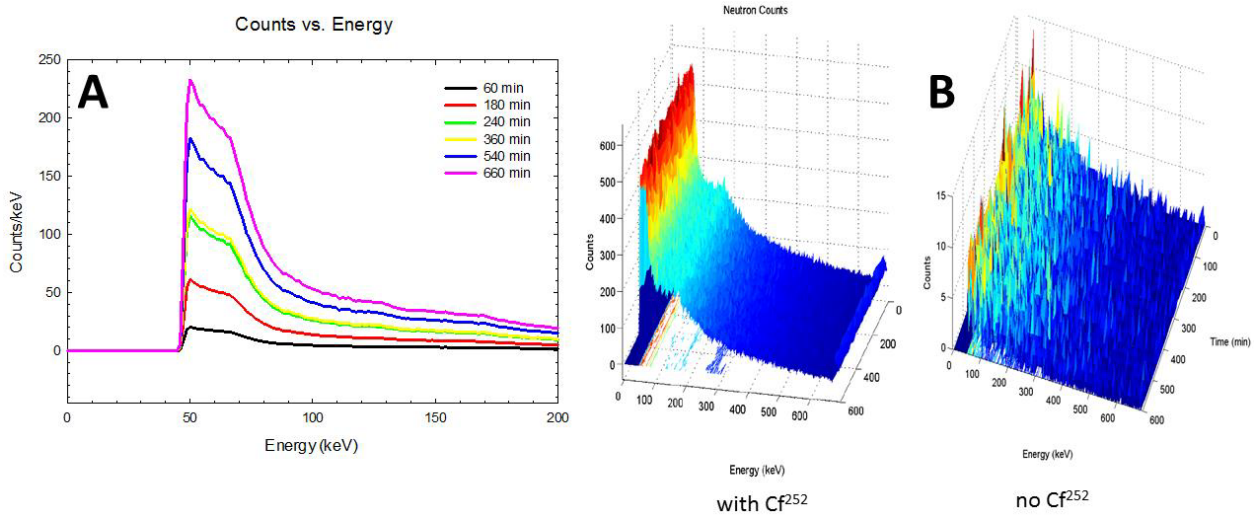

Figure 4. Energy spectrum (A) and signal/background (B) from Gd conversion material. Both X-rays and electrons are visible in the energy spectrum. In panel B, the background-subtracted ICE from neutron capture in natural Gd is shown.

depositing uniform Gd films directly onto the diode contributed to overall improvements in efficiency.[35]

Gd Emission Spectrum:

A spectrum recorded from the charged particle detector is shown in Figure 4A with peaks at various energy levels due to electrons and X-rays. Clearly visible in the profile are the K_α X-ray at 43 keV along with three ICE at ~72, 131 and 174 keV over collection times of 1-10 hours. Under these conditions, a signal/background (S/B) of 40 was obtained (Figure 4B). The plot (Figure 4A) is calculated by first finding the difference in the running average of the signal (μ_{Cf}) to baseline (μ_B) for a series (*m*-*n*) of data records and then finding the average counts at that energy over the period of averaging. The data are then divided as a function of energy to arrive

at the counts/energy data plotted in Fig. 4A. The algorithm is written mathematically as the following:

$$\left.\frac{C}{E}\right|_n = \frac{\left[\frac{\sum_{k=1}^{N}\left(\sum_{j=n}^{m}\mu_{Cf}(E_n) - \sum_{j=n}^{m}\mu_B(E_n)\right)_k}{N}\right]}{E_n} \qquad \backslash* \text{ MERGEFORMAT (3)}$$

where the ratio of the counts/energy in any "bin" n is given in Eq. * MERGEFORMAT (3).

By measuring the spectrum, even low neutron fluxes from solid-state devices could be detected in an architecture that was capable of being miniaturized for personal, wearable and field monitoring applications.

In order to obtain a clean electron spectrum, ICE was blocked using aluminum foil, enabling subtraction of the background to yield the electron foreground (Figure 5A) and study cross-sensitivity, where Al was blocking electrons below 100 keV (Fig. 5B).[42,43] The majority of

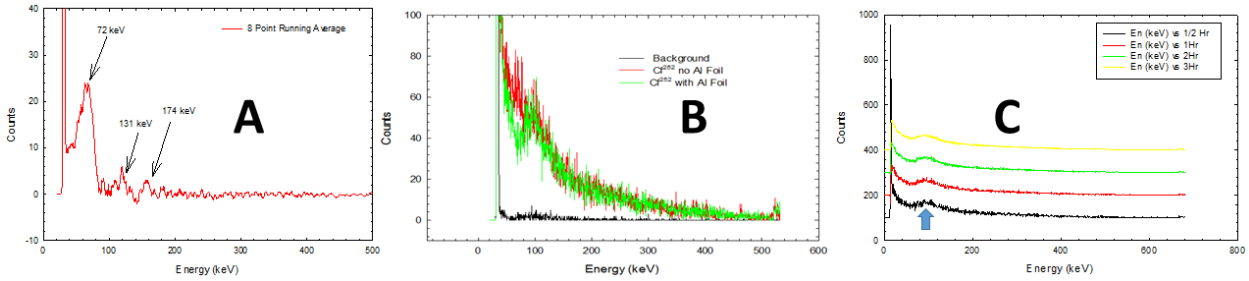

Figure 5. Panel A shows the clean electron spectrum with aluminum foil shielding, from four hours, 8 points running average measurements. A PD300-16-100AM 100 µm thick diode was the detector. In panel B, the Al foil is placed above the Gd film and is shorted to the chassis during the experiment. The difference data is the four hours of accumulation of all the scans with four points running average and illustrates the three peaks expected from the electrons. The calibration is slightly off due to uncertainties in the calibration procedure. In panel C, the specificity of X-ray and ICE peaks (blue arrow) at 0.5-3 hours are shown. There is a vertical offset of 100 counts for each integration time point for visualization. Average counts per energy bin with background subtraction are reported using the same diode.

ICE had an energy of ~72 keV from the *L*-shell of ^{158}Gd and these were the principal electron-hole pair producers in the semiconductor. This broad peak was due to the electrons losing some energy during transit through the Gd film. Another option is a window discriminator (40-100 keV) to electronically filter electrons, such as those produced by γ-ray, with energies outside this range.[33] Other electron peaks were at 131 keV and 174 keV energies, from *K* and *L* shell electrons de-excitation of the 181.9 keV nuclear level of ^{158}Gd (Figure 5A). Missing from this spectrum are 29 keV ICE from the de-excitation of 79 keV *K*-shell electrons of ^{158}Gd (expected

~20% of the time). This could be due to the 25-30 keV setting of lower-level discriminator (LLD), to reduce noise. The 29 keV conversion electrons would lose energy as they travelled through the foil and therefore were not detected. There were also no ICE from the de-excitation of ^{156}Gd, attributed to low-abundance relative to ^{158}Gd ICE. Longer collection times might reveal these. Bias scaling was performed using a 100 µm thick diode with calibration at each bias for optimization, and the data yielded adequate S/B of 4.0 at 30 min. collection point with high specificity at low flux (Figure 5C). Reverse biasing of the detector by an external applied voltage improves charge collection by increasing the width of the depletion layer and decreasing electrical noise.[33] Clearly collection times were very long; therefore the focus shifted towards optimizing the Gd film thickness to improve neutron capture and maximize ICE generation.

Optimizing Gd Thickness

The Si semiconductor has a cross-section of ~2.24 barns for thermal neutrons and an effective mean free path of ~8.6 cm, making neutron detection using Si alone nearly impossible. For this reason, Gd converter layer was used (Figure 1). In the planar diode configuration (Figure 1), due to its high cross-section, a thin layer of Gd was used to create charged particles that escaped this layer and were detected as electronic pulses. If the conversion layer was too thick, the ICE might not have sufficient energy to escape and reach the detector volume for electron-hole pair

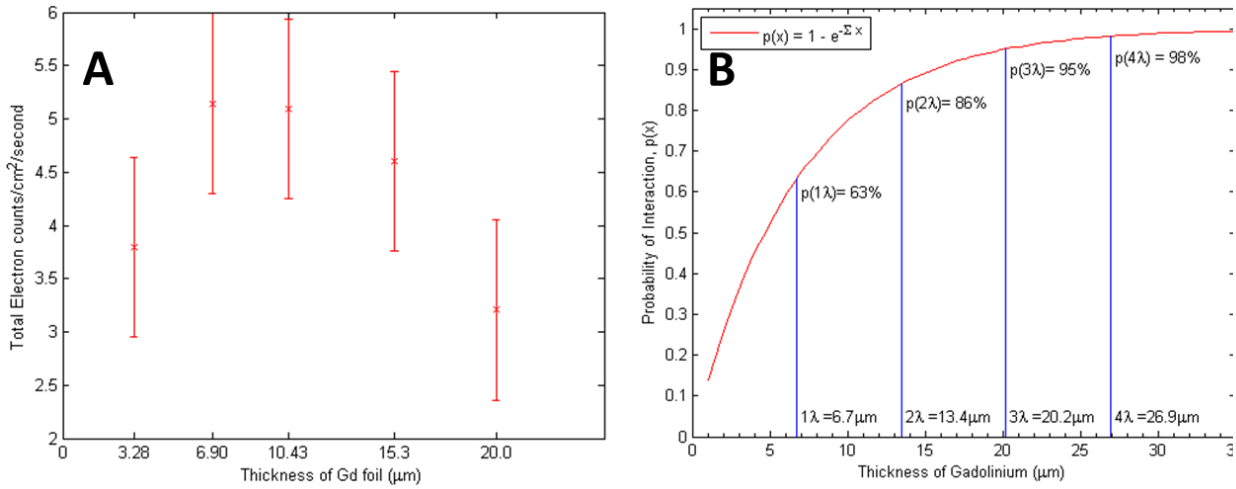

Figure 6. Optimization of Gd film thickness. Panel A shows the Gd film optimization determined experimentally using conversion electron count rate from neutron capture in natural Gd at multiple film thicknesses. Panel B shows the probability of neutron capture in natural Gd as determined theoretically. Probability is shown explicitly at 1 (6.7 µm), 2 (13.4 µm), 3 (20.2 µm), and 4 (26.9 µm) mean free paths.

generation. A thinner Gd layer might not capture thermal neutrons efficiently.[36] The goal was to identify a Gd conversion layer thickness that maximized neutron capture whilst simultaneously having the highest ICE escape potential.

The optimum Gd thickness was calculated based on the reaction cross-section, Gd density, and the range of ICE. Due to gadolinium's large cross-section, a 50 µm film will be completely opaque to thermal neutrons; however, none of the ICE will have sufficient escape energy. The

cross-section of 255,000 barns for ^{157}Gd translates into a mean free path of 1.3 μm for thermal neutrons. Thus, a 6.0 μm Gd layer will stop ~99% of neutrons. With natural Gd used here, a 5 μm film will allow ICE to escape, but might not result in maximum neutron capture. The mean free path of a thermal neutron in natural Gd is ~7 μm, whereas the range of 72 keV ICE is >20 μm. Therefore, a 7-10 μm thick Gd layer will absorb ~80% of incident thermal neutrons, and the ICE will still have sufficient escape energy. The optimum conversion layer thickness was determined experimentally by correlating ICE count-rate as a function of Gd foil thickness (Figure 6). Results confirmed that the maximum count-rate was indeed between 7-10 μm. Film thicknesses flanking these values had lower count rates indicative of either low neutron capture (3.3 μm) or fewer ICE having sufficient escape energy (15.3 μm and 20 μm) (Figure 6A). The experimental data agreed with theoretical calculations. Using a mean free path value of 6.7 μm for thermal neutron, the probability of interaction, *p*, is given by the following equation:

$$p(x) = \int_0^x \sum_a e^{-\sum_a x'dx'} = 1 - e^{-\sum_a x} \qquad \text{* MERGEFORMAT (4)}$$

where *x* is the thickness of the material traversed by neutrons. When Eq. * MERGEFORMAT (4) was profiled as a function of natural Gd thickness, the probability of a neutron absorption in 1, 2, 3, and 4 mean free paths could be determined (Figure 6B). Results showed that ~80% probability of interaction determined theoretically (Figure 6B) was also at 10 μm as determined empirically (Figure 6A). Although the probability of interaction increased slightly at higher thicknesses (Figure 6B), the escape potential of conversion electrons decreased over this range (Figure 6A). All further experiments were therefore carried out using 10 μm Gd layers which was also close to the 12 μm predicted previously for natural Gd to achieve high efficiency of ~32%.[31]

Diode Thickness

A 300 μm thick diode gave the best sensitivity for neutron detection (Figure 6). There were several considerations in determining the optimum depletion layer thickness. The bandgap in Si of 1.11 eV results in an average energy of 3.6 keV for electron-hole creation.[35] A minimum ionizing particle (MIP) creates on average 24,500 electron equivalents in a 300 μm thick diode [33], enabling the measurement of a charge of less than 5000 electrons from the low energy ICE.[35] The present choice of 300 μm diode was consistent with literature reports that large depletion layers are preferable during ICE measurements.[37]

Detection Speed

The time resolution is governed by a number of parameters. These included the charge collection time in Si, transit time for thermal neutrons through Gd film, and the lifetime of excited Gd atoms after neutron capture.[35] All these time scales are on the order of a few nanoseconds. For example, in the 300 μm diode operated at -100 V bias (Figure 7), electrons and holes are collected in about 8 *ns* and 21 *ns*, respectively.[33] Thus, the rate-limiting step is the readout electronics.[33, 35] The detection speed improved dramatically following the use of optimized Gd film detectors and the data are presented in Fig. 7. All three dominant ICE energies, namely

72 keV, 132 keV, and 174 keV, were detected using the optimized detector within 30 minutes (Figure 7A) and subsequently at 10 minutes (Figure 7B), although the signal intensity at 10 minutes was weaker, but nevertheless clearly discriminated. The signal intensity also tracked linearly with integration time, as seen by a three-fold decrease in the counts for 72 keV ICE at 10 minutes (Figure 7B) compared to 30 minutes integration (Figure 7A). This timescale fits reasonably with the notion that a 20-foot container is likely to be scanned in 10 minutes, but it is still not within time limits for port-of-entry detection of SNM, where containers are driven at 4-5

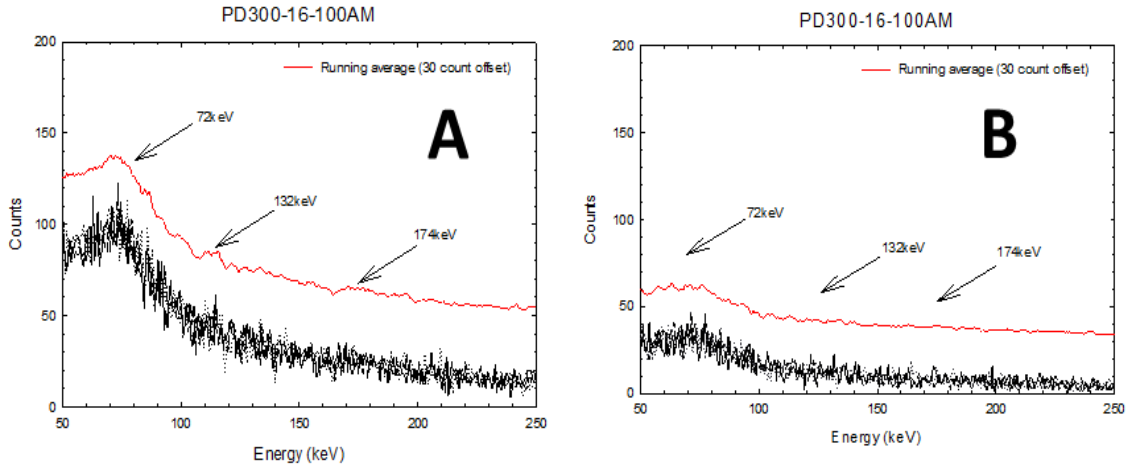

Figure 7. Panel A shows the profile of four replicates of a 30 min. integration time. The red line is a running average of the data and demonstrates the ability to clearly resolve the 72 keV, 132 keV, and 174 keV electrons produced by the moderated electron interaction with the natural Gd film. Panel B shows four replicates of a 10 min. integration time. The remainder of the details are the same as in panel A. The diode used in both experiments was the same and indicated on top of the panels. The running averages are offset for clarity by adding 30 counts to separate them from the raw data.

miles per hour passing through a radiation portal monitor (RPM) equipped with passive polyvinyl toluene (PVT) γ-ray scanners in about 20 seconds.[38] The 10 minute detection window (Figure 7B) is within striking distance of the requirement for two-minute scan per 40-foot containers.[39] The present detection time could be improved by decreasing/eliminating the air-gap (Figure 1) and implementing other optimization steps. Alternately, the present detector configuration could be used as a confirmatory test for SNM after PVT alerting of suspicious cargo. Another possibility is to use the current detector for random cargo screening that currently accounts for <0.5% of incoming containers,[38] and where scanning speed is not an overwhelming concern.

Modeling and Efficiency Calculations

Detector efficiency is governed by a series of probabilities for certain events. These include the probability that a neutron will be captured by a Gd converter, that every captured neutron will result in an electron emission, the escape probability of electron from the Gd layer and finally, probability of the escaped electron reaching the detector volume in order to produce a signal.[35] Experimental results were modeled using the Monte Carlo code (GEANT4) with excellent

correlation to the production of ICE. The charged particle detector was modeled as a thin, 500 μm layer of Si, located directly above the Gd film. A successful simulation was demonstrated from the remarkable overlap of the modeling spectrum with experimental spectra (Figure 4A and Figure 5A) with clear evidence of ICE at 70 keV along with γ-rays from neutron capture, and K_α X-rays at 43 keV in the simulation spectra.

Figure 6A shows the the GEANT4 modeled electron count rate/area/time for the experimental system as assembled. For the 10 μm films that we tested, we expect signal from ICE of around 5 electrons/(cm^2 sec). Examination of Figure 5A, it is observed that total integrated charge measured by the detector during the Al blocking experiment is approximately 450 electrons. Since the system was configured to integrate charge over a 4 hr (14400 sec) time interval, the detector has efficiency on the order of ε=0.002 for a 300 mm^2 area detector. This efficiency is very small as measured; however, the geometry of the measurement system (Figure 1) alludes to the approximately 1 cm separation between the detector and the Gd film.

A significant improvement in electron capture efficiency should be possible moving the film into contact with the diode surface. This is observed in Figure 7 where a total integrated charge over a 2 hr interval was measured and approximately 78000 electrons were counted from a 10 μm coated detector. This results in an efficiency that is estimated to be ε=0.4 or an improvement of about 200 times. The above efficiencies are really electron capture efficiencies of the coated and uncoated device.

An efficiency number that we will refer to the system efficiency is defined as the number of electrons counted/sec (10.8/sec) divided by the number of neutrons incident on the detector/sec. For simplicity, we will assume a point Cf source at a distance of r=15 cm from the detector. The system efficiency can be calculated as shown below where the subscripts *det* and *source* refer to the rates at the detector and source respectively, and $A_{det}=300\ mm^2$.:

$$\varepsilon_{sys} = \frac{\dot{N}_{det}}{\dot{n}_{det}} = \frac{\dot{N}_{det}}{\frac{A_{det}}{4\pi r^2}\dot{n}_{source}} \qquad \text{* MERGEFORMAT (5)}$$

We report a system efficiency of about ε_{sys}=0.07.

4. CONCLUDING REMARKS

The solid state detector described here offers advantages over competing technologies. For example, boron-10 (^{10}B) neutron capture cross-section is 3840 barns, similar to ^{3}He and an order-of-magnitude lower than natural Gd, leading to ~2.3-fold higher energy deposition rate with the latter.[1, 36, 40, 41] The 2 MeV α-particle from the ^{10}B reaction has a range of 3.4 μm and the ^{6}Li nucleus has an even shorter range.[33] The mean free path for thermal neutrons in ^{10}B is ~20 μm. These conflicting factors reduce the efficiency to ~6%.[35] On the other hand, Gd capture cross-section extends up to 200 MeV, relative to ^{10}B neutron energy moderation of 25-30 MeV.[1] The mean free path of thermal neutrons in Gd is 6.785 μm and the range of 72 keV ICE is >20 μm. Thus, Gd converter layers could be made thin and still capture ~95% of thermal neutrons with ICE still having sufficient escape energy.[35] Unlike ^{10}B, ^{6}Li or ^{3}He neutron detectors, solid-state Gd-based sensors do not produce massively charged α-particles that could interfere with detector electronics/software, degrade long-term sensor performance, or pose safety hazards.[31, 41] Therefore, the emphasis is on low-damage electron products rather than α-particles.

In addition to the ^{3}He shortage, tube detectors are bulky, suffering from configuration, portability, and field deployment issues. The high-pressure ^{3}He makes transport difficult and high-voltage bias is hazardous for under-water operations. System stability is poor due to microphonics (mechanical vibrations producing electrical noise) sensitivity and bumping the system could produce false positives. Solid-state neutron detectors can be mass-produced, are compact for portability and wearability for personal/field monitoring, and can operate on a few volts without requiring high-power.[37] Planar semiconductor detectors are a straightforward configuration for fixed or mobile neutron monitoring due to advantages of size, sensitivity, weight, power consumption, safety, transportability, and manufacturing cost, where conventional wafer level device fabrication is possible for high throughput.[28]

5. FUNDING

These investigations were supported by Sandia's Laboratory Directed Research and Development (LDRD) project # 176117.

6. REFERENCES

1. Santana, J.A.C., et al., *Gamma and X-ray sensitivity of GdO3 heterojunctions.* Radiation Measurements, 2013. **51-52**: p. 99-102.

2. Ovechkina, L., et al., *Gadolinium loaded plastic scintillators for high efficiency neutron detection.* Phys. Procedia, 2009. **2**: p. 161-170.

3. Maruyama, Y., J.M. Feola, and J.L. Beach, *A tumor/normal tissue advantage for low dose rate neutron brachytherapy.* Int. J. Radiat. Oncol. Biol. Phys., 1983. **9**(11): p. 1715-1721.

4. Ishikawa, M., et al., *Application of an ultraminiature thermal neutron monitor for irradiation field study of accelerator-based neutron capture therapy.* J. Radiat. Res., 2015. **56**: p. 391-396.

5. Masunaga, S.I. and K. Ono, *Significance of the response of quiescent cell populations within solid tumors in cancer therapy.* J. Radiat. Res., 2002. **43**: p. 11-25.

6. Cerullo, N., D. Bufalino, and G. Daquino, *Progress in the use of gadolinium for NCT.* Appl. Radiat. Isotopes, 2009. **67**: p. S157-S160.

7. Enger, S.A., et al., *Dosimetry for gadolinium nuetron capture therapy (GdNCT).* Radiation Measurements, 2013. **59**: p. 233-240.

8. Beni, M.S., et al., *A calibration method for realistic neutron dosimetry in radiobiological experiments assisted by MCNP simulation.* J. Radiat. Res., 2016. **July 5**(doi: 10.1093/jrr/rrw063): p. 1-7.

9. Ng, C.Y.P., et al., *Non-induction of radioadaptive response in zebrafish embryos by neutrons.* J. Radiat. Res., 2016. **57**(3): p. 210-219.

10. Romanyukha, A., D.L. King, and L.K. Kennemur, *Impact of the Fukushima nuclear accident on background radiation doses measured by control dosimeters in Japan.* Health Phys., 2012. **102**(5): p. 535-541.

11. Imanaka, T., *Transport calculation of neutrons leaked to the surroundings of the facilities by the JCO criticality accident in Tokai-mura.* J. Radiat. Res., 2001. **42**(Suppl.): p. S31-S44.

12. Straume, T., et al., *Emerging technological bases for retrospective dosimetry.* Stem Cells, 1997. **15**(S1): p. 183-193.

13. Shizuma, K., et al., *Measurement of residual 60Co activity induced by atomic-bomb neutrons in Nagasaki and background contribution by environmental neutrons.* J. Radiat. Res., 2002. **43**: p. 387-396.

14. Pugliesi, F., et al., *The feasibility of polycarbonate Duralon as a thermal neutron dosimeter.* Appl. Radiat. Isotopes, 2014. **89**: p. 1-5.

15. Endo, S., et al., *Dosimetry of fission neutrons in a 1-W reactor, UTR-KINKI.* J. Radiat. Res., 2002. **43**: p. 381-386.

16. Maeyama, T., et al., *Radiological properties of nanocomposite Fricke gel dosimeters for heavy ion beams.* J. Radiat. Res., 2016. **57**(3): p. 318-324.

17. Maruyama, Y., et al., *Californium Cf-252 for pelvic radiotherapy.* Oncology, 1978. **35**(4): p. 172-178.

18. Wang, C.K.C., *Progress in californium-252 neutron brachytherapy.* Brachytherapy, 2012. **Chapter 3**: p. 33-58.

19. Martin, R.C., J.B. Knauer, and P.A. Balo, *Production, distribution and applications of californium-252 neutron sources.* Appl. Radiat. Isotopes, 2000. **53**: p. 785-792.

20. Wierzbicki, J.G., M.J. Rivard, and W. Roberts, *Physics and dosimetry of clinical 252Cf sources.* Californium-252 isotope for 21st century radiotherapy, 1997. **29**: p. 25-53.

21. Huang, K.C., et al., *Scalable large-area solid-state neutron detector with continuous p-n junction and extremely low leakage current.* Nucl. Instrum. Meth. Phys. Res. A, 2014. **763**: p. 260-265.

22. Maurya, D.K., A. Sardarinejad, and K. Alameh, *Recent developments in R.F. Magnetron sputtered thin films for pH sensing applications - an overview.* Coatings, 2014. **4**: p. 756-771.

23. Allison, J., et al., *Geant4 developments and applications.* IEEE Transactions on Nuclear Science, 2006. **53**(1): p. 270-278.

24. Ramirez-Jimenez, F.J., L. Mondragon-Contreras, and P. Cruz-Estrada, *Application of PIN diodes in physics research.* AIP Conf. Proc. **857**: p. 395-406.

25. Abdushukurov, D.A., *Gadolinium foils as converters of thermal neutrons in detectors of nuclear radiation.* Nova Science Publishers, Inc., 2008. **New York**: p. 37.

26. Eijk, C.W.E.v., *Neutron detection and neutron dosimetry.* Rad. Protec. Dosimetry, 2004. **110**(1-4): p. 5-13.

27. Varner, R.L., J.R. Beene, and P.S. Friedman, *Gadolinium foils in a plasma panel sensor as an alternative to 3He.* IEEE Nuclear Sci. Symp. Med. Imaging Conf., 2010. **Oct 30-Nov 6**: p. 1130-1136.

28. McGregor, D.S., et al., *Recent results from thin-film-coated semiconductor neutron detectors.* Proc. SPIE, 2002. **4784**: p. 164-182.

29. Malhotra, R. and Y.B. Gianchandani, *A microdischarge-based neutron radiation detector utilizing sputtered gadolinium films for neutron conversion.* IEEE Sensors J, 2015. **15**(7): p. 3863-3870.

30. Duygulu, N.E., A.O. Kodolbas, and A. Ekerim, *Effects of argon pressure and r.f. power on magnetron sputtered aluminum doped ZnO thin films.* J. Crystal Growth, 2014. **394**: p. 116-125.

31. Kandlakunta, P. and L. Cao, *Gamma-ray rejection, or detection, with gadolinium as a converter.* Rad. Protec. Dosimetry, 2012. **151**(3): p. 586-590.

32. Caruso, A.N., *The physics of solid-state neutron detector materials and geometries.* J. Phys. Condens. Matter, 2010. **22**: p. 443201 (32 pp).

33. Petrillo, C., et al., *Solid state neutron detectors.* Nucl. Instrum. Meth. Phys. Res. A, 1996. **378**: p. 541-551.

34. Gualdrini, G., et al., *Analysis of the Conrad computational problems expressing only stochastic uncertainties: neutrons, and protons.* Rad. Protec. Dosimetry, 2008. **131**(1): p. 7-14.

35. Bruckner, G., et al., *Position sensitive detection of thermal neutrons with solid state detectors (GdSi planar-detectors.* Nucl. Instrum. Meth. Phys. Res. A, 1999. **424**: p. 183-189.

36. Kandlakunta, P. and L.R. Cao, *Neutron conversion efficiency and gamma interference with gadolinium.* J. Radioanal. Nucl. Chem., 2014. **300**: p. 953-961.

37. Schulte, R.L., F. Swanson, and M. Kesselman, *The use of large area silicon sensors for thermal neutron detection.* Nucl. Instrum. Meth. Phys. Res. A, 1994. **353**: p. 123-127.

38. Dalal, S.R. and B. Han, *Detection of radioactive material entering national ports: A Bayesian approach to radiation portal data.* Ann. Appl. Statistics, 2010. **4**(3): p. 1256-1271.

39. Rose, P.B., et al., *Uncovering special nuclear materials by low-energy nuclear reaction imaging.* Nature Scientific Reports, 2016. **6:24388**(DOI: 10.1038/srep24388): p. 1-8.

40. Kandlakunta, P., L.R. Cao, and P. Mulligan, *Measurement of internal conversion electrons from Gd neutron capture.* Nucl. Instrum. Meth. Phys. Res. A, 2013. **705**: p. 36-41.

41. Lee, N.H., et al., *Development of a pMOSFET sensor with a Gd converter for low energy neutron dosimetry.* Rad. Protec. Dosimetry, 2004. **110**(1-4): p. 277-281.

42. R. Wagner, S. Y. Chen, A. Maksimchuk, and D. Umstadter, *Electron acceleration by a laser Wakefield in a relativistically self-guided channel,* Phys. Rev. Lett., 1997, 78: p. 3125-3128.

43. D. Umstadter, S. Y. Chen, R. Wagner, A. Maksimchuk, and G. Sarkisov, *Nonlinear optics in relativistic plasmas,* Optics Exp., 1997: 72: 282-288.

7. DISTRIBUTION

1	MS0382	M. L. B. Denton	2121
3	MS0892	R. P. Manginell	1714
1	MS0966	P. L. Dreike	5700
1	MS1072	E. I Cole	1000
1	MS1202	R. S. Bennett	5957
1	MS1202	C. A. Coverdale	5857
1	MS1209	M. C. Jackson	5950
1	MS1218	M. Allen	5942
2	MS1415	M. P. Siegal	1124
3	MS1425	K. B. Pfeifer	1714
1	MS1425	Komandoor Achythan	1714
1	MS0899	Technical Library	9536 (electronic copy)
1	MS0359	D. Chavez, LDRD Office	1911
1	MS0161	Legal Technology Transfer Center	11500


Sandia National Laboratories